Monitoring horizontal and vertical surface deformation over a hydrocarbon reservoir by PSInSAR

Hanno Klemm,[1*] Issa Quseimi,[2] Fabrizio Novali,[3] Alessandro Ferretti[3] and Andrea Tamburini[3]

Abstract

We study surface deformation monitoring over a hydrocarbon reservoir in the Middle East with permanent scatterer interferometric synthetic aperture radar (PSInSAR). By combining data from two different observation angles, it is possible to disentangle horizontal and vertical deformation of the Earth's surface. We benchmark the PSInSAR data against an existing GPS network and find good agreement in both vertical and horizontal displacements. In order to relate the surface data to the reservoir, we invert the surface deformations using an analytical geomechanical model and obtain reservoir strain. Assuming linear poroelasticity, we relate the strain to pressure depletion. The areal extent of the reservoir strain is in good agreement with predictions from reservoir simulation. By considering velocity gradient maps, we find intriguing relationships between major faults in the reservoir and the surface data. We conclude that surface deformation monitoring and geomechanical inversion can provide valuable information on dynamic reservoir behaviour.

Introduction

Surface deformation monitoring can provide valuable information about the dynamic behaviour of reservoirs under production. Compacting reservoirs induce surface subsidence, as well as contraction (Figure 1). Measuring these deformations can identify undepleted compartments, detect fault reactivation, mitigate risks associated with well failure, constrain geomechanical models, and aid field management decisions. Furthermore, surface subsidence monitoring is, in some countries, a legal requirement for hydrocarbon extraction.

Some examples where surface deformation monitoring has realized value are the Belridge and Lost Hills fields in California (Patzek and Silin, 2000; Patzek et al., 2001; van der Kooij and Mayer, 2002), the cyclic steam injection trial in Peace River Pad 40 (Maron et al., 2008), and the $C0_2$ sequestration trial in In Salah, Algeria (Raikes et al., 2008; Vasco et al., 2008). The technologies that are most often used for surface deformation monitoring are GPS, optical levelling, tiltmeter, and satellite radar interferometry. Of these technologies, only interferometric synthetic aperture radar (InSAR) using satellites provides the possibility of acquiring full areal coverage over the area of interest with a data point every few metres. The distance of neighbouring measurement points for all other technologies is of the order of hundreds to thousands of metres, and the actual measurements have to be interpolated to obtain a displacement field. This can lead to the possibility that features with a shorter length scale might not be captured.

We present a study of permanent scatterer InSAR (PSInSAR) data over a stacked carbonate reservoir in the Middle East. The top reservoir is a mature gas reservoir at a depth of approximately 750 m, which is known to compact. The lower reservoir is an oil reservoir at 1200 m depth that is produced by water-flood. Both reservoirs are intersected by a major graben fault, trending NE-SW, as well as numerous additional extensional faults. Approximately 500 producer

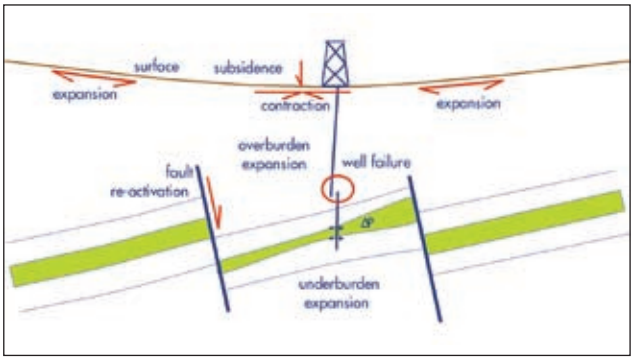

Figure 1 *Geomechanical effects of a depleting reservoir. Reservoir depletion might lead to surface subsidence, accompanied by horizontal movements of the surface. It might induce fault reactivation which can lead to well failure or damage to surface facilities.*

[1] *Shell International Exploration & Production, 2280 GS Rijswijk, Netherlands.*
[2] *Petroleum Development Oman, Mina al Fahal, Muscat, Oman.*
[3] *Tele-Rivelamento Europa, Via Vittoria Colonna 7, 20149 Milano, Italy.*
**Corresponding author, E-mail: hanno.klemm@shell.com*

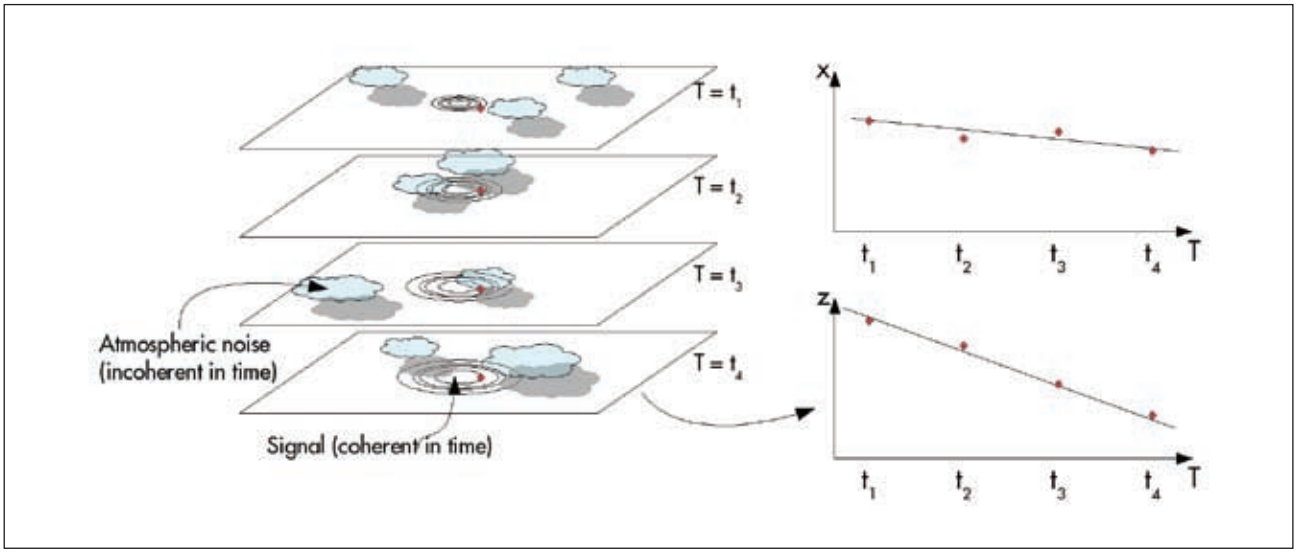

Figure 2 *Concept of PSInSAR processing. At regular intervals, SAR images of the surface are recorded. Points on the surface that exhibit coherent behaviour in time are identified and their motion is tracked. By using a motion model, the temporally coherent part of the motion is disentangled from atmospheric fluctuations which are random in time.*

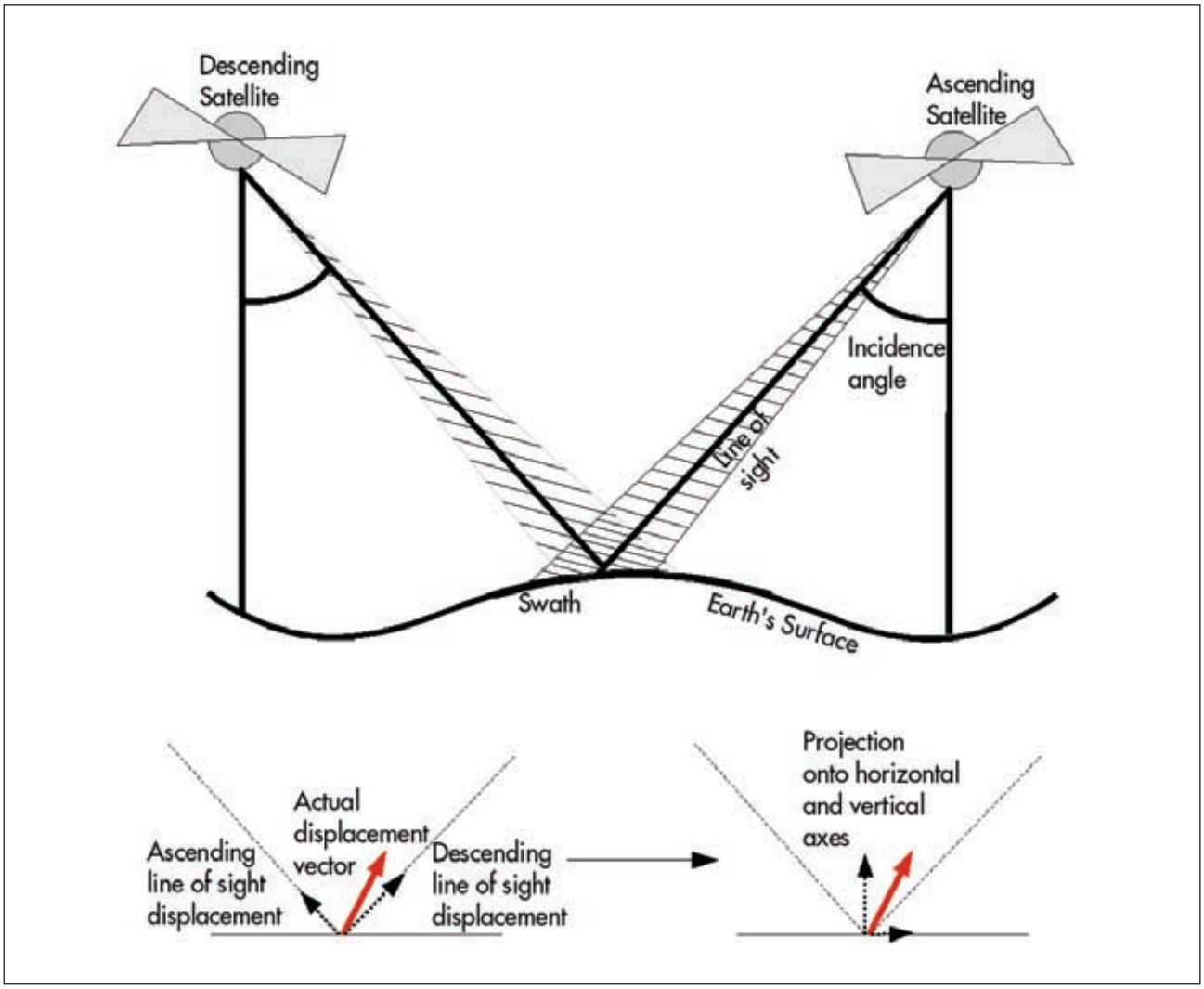

Figure 3 *The horizontal and vertical components of displacement can be distinguished by using measurements from different observation angles.*

and injector wells have been drilled in the area, so mitigating large-scale well failure is a business driver. We show that PSInSAR is a powerful tool to image surface subsidence. By comparing the PSInSAR results with the measurements of an existing GPS network, we obtain estimates of the reliability of the results. Using a geomechanical model we invert the PSInSAR data to obtain reservoir strains, which compare well with pressure change maps from reservoir simulations. We note an intriguing correlation between known fault systems at reservoir level and the surface data.

Monitoring technology

In this section we give a brief overview of PSInSAR technology. A synthetic aperture radar (SAR) satellite sends out a radar pulse, and the phase and the amplitude of the backscattered signal from the Earth's surface are subsequently recorded. InSAR uses the phase differences between two SAR acquisitions to obtain interferograms (Madsen and Zebker, 1998; Hanssen, 2001). These phase difference observations are used to estimate ground motion, but also contain contributions due to topographic heights, atmospheric signal, and slight deviations of the satellite's orbit.

For conventional InSAR processing, an interferogram is formed from two SAR images. After removal of the influences of the terrain heights, the interferogram represents primarily surface deformation and atmospheric disturbances. This processing technique has the disadvantage that the atmospheric phase screen (atmospheric distortions) cannot be estimated reliably.

For PSInSAR processing, phase changes in a series of SAR images acquired at different times over the same area are analysed (Ferretti et al., 2001). One image is selected as the master image and interferograms between the master image and all other images of the series are formed. Within this stack of interferograms, pixels exhibiting coherent phase behaviour in time are identified. These targets are so-called permanent scatterers (PS). They form a network of measurement points from which surface deformation, topographic heights, and error sources, such as atmospheric signal, can be estimated. In PSInSAR, atmospheric artefacts can be suppressed more effectively compared to conventional InSAR, thanks to the use of a long series of interferograms. The atmospheric phase screens of all acquisitions are estimated and removed, based on the assumption that the atmosphere is correlated in space but not in time (Figure 2). The estimation procedure results in a time series of PS displacements that describe the actual movements of the permanent scatterers in the satellite line-of-sight.

Permanent scatterers are often man-made structures, such as roofs, streets, and pipelines. In vegetated areas, few permanent scatterers may be found. Deformation estimates obtained from InSAR observations are along the satellite line-of-sight. For different acquisition modes, the incidence angle varies from ~23° to ~45° between the vertical and horizontal east-west direction. The same point on the Earth's surface can be viewed from multiple satellite positions in space, as the recorded areas are overlapping for adjacent tracks. Furthermore, the satellite can image the same spot, once heading from the South Pole to the North Pole and a second time heading from the North Pole to the South Pole. These directions are called *ascending* and *descending*. Ascending and descending acquisition geometries can image the same area once looking 'from the east' and once looking 'from the west'. By combining an ascending and a descending time-series, it is possible to disentangle east–west horizontal deformation from vertical deformation (Figure 3). As a new SAR image is available every 11–35 days, depending on the satellite, it is possible to track deformation in time and therefore improve the understanding of the temporal developments of the sources of the deformation.

Data and benchmarking

For this study, one ascending and one descending dataset have been acquired over the time period 2004–2007. The ascending time series was acquired by the European Space Agency (ESA) *Envisat* satellite, and comprises 20 images acquired with a 35-day repeat pass, while the descending dataset was acquired by the Canadian Space Agency (CSA) satellite *Radarsat-1* and comprises 34 images, acquired with a 24-day repeat pass. In Figures 4 and 5, the estimated average displacement rates along the satellite lines-of-sight (LOS) are shown. The high scatterer density shows that the area is well suited for PSInSAR monitoring. With Envisat, it was possible to extract more than 280,000 PS, and with Radarsat more than 360,000 PS could be identified. This corresponds to a scatterer density of about 2400 and 3000 PS km^{-2}, respectively.

In order to extract the horizontal and vertical components of the deformation, PS data were first gridded on a 50 m × 50 m grid and the results for scatterers falling within the same grid cell were averaged. This step was necessary since the backscattered signals for the ascending and descending geometry do not necessarily originate from the same scatterer. Furthermore, the time series of deformation had to be resampled over time on to a regular 20-day interval, as the data acquisition intervals for the two satellites is different. The resulting average vertical and horizontal displacement rates are shown in Figures 6 and 7.

Figure 6 shows a subsidence bowl with a smaller depression to the northeast, and Figure 7 shows that the scatterers move inwards, as expected. In the southeast corner of the field, a feature that is rising, rather than subsiding, can be identified. The area has the form of an inverted y. Here, the temporal resolution of PSInSAR data provides additional insight, as it shows that the first area to start rising was the northernmost part of the structure, labelled by 1 in Figure 8. Only later, the areas 2 and 3 start

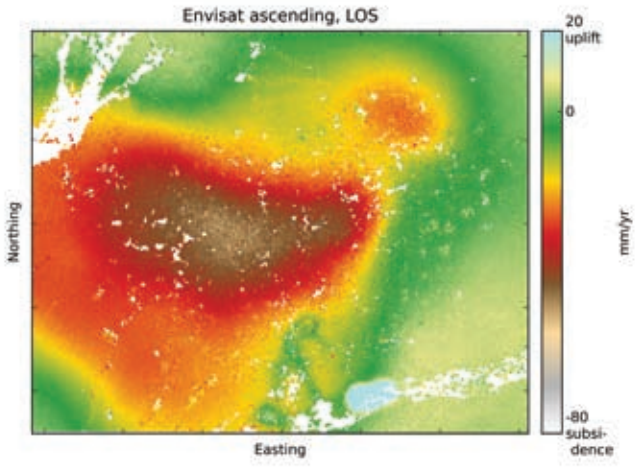

Figure 4 *Average displacement rates along the line-of-sight of Envisat. Tick marks on eastings and northings are at 2 km intervals.*

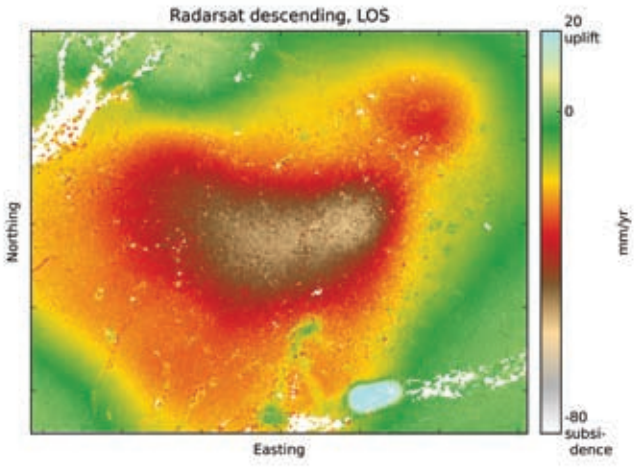

Figure 5 *Average displacement rates along the line-of-sight of Radarsat.*

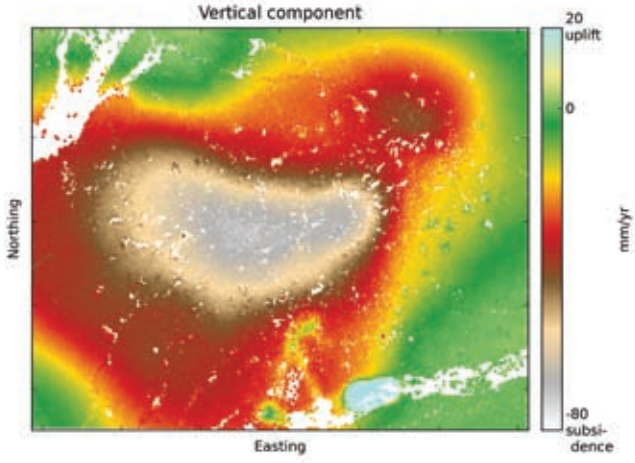

Figure 6 *Vertical component of surface deformation as derived from the Radarsat and Envisat time series.*

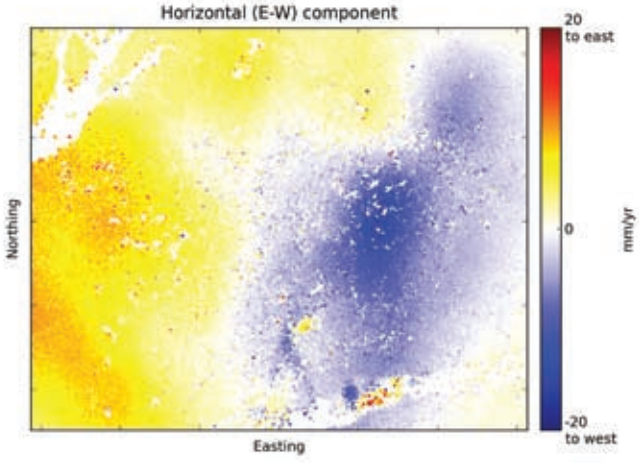

Figure 7 *Horizontal component of surface deformation as derived from the Radarsat and Envisat time series.*

rising. The strong uplift at area 3 has been attributed to water collecting above a shallow impermeable layer. The uplift in area 1 has been associated with a corroded water injection well that injected into a shallow aquifer rather than into the oil reservoir.

Subsidence over this field is also being monitored by GPS and optical levelling, which provides a good opportunity to assess the deformation rate estimates from PSInSAR against the deformation rates measured by GPS. A permanent GPS network is installed over the field, and the measured subsidence rates of GPS and optical levelling agree within their respective errors. The GPS network was designed, and the data are being analysed, by MIT. For details on the methodology, see Herring (1999, 2003). The formal error of the optical levelling campaigns on the subsidence rates are 0.8–5.6 mm yr^{-1} and the formal errors of GPS are 1.5–2.7 mm yr^{-1} in the horizontal direction and 2.0–2.9 mm yr^{-1} in the vertical direction.

In order to establish a benchmark for the quality of the predicted time series, we compare the subsidence rates measured by GPS to the subsidence rates measured by PSInSAR. The average of the deformation time series in a radius of 100 m was compared to the GPS measurements at 39 locations (Figure 9). The subsidence rates at the comparison stations have a range between zero and 6 cm yr^{-1} of vertical deformation, and between +10 and –10 mm yr^{-1} horizontal deformation, where movement to the east is counted as positive. Both InSAR and GPS measurements are relative measurements against some reference point which is assumed to be fixed. However, the GPS reference station is situated outside the area captured by the InSAR analysis. Therefore, we used an arbitrary GPS station within the area of interest as the reference station and only considered relative differences between the measurements. Figures 10 and 11 show the crossplot of GPS and InSAR displacement rates for both components, as well as histograms of the residuals. The horizontal deformations agree within 1.8 mm yr^{-1}, while the vertical deformation rates agree within 4.8 mm yr^{-1}. In particular, the agreement in the horizontal component is close to the error budget of the GPS predictions and thus shows excellent agreement. The differences in the standard

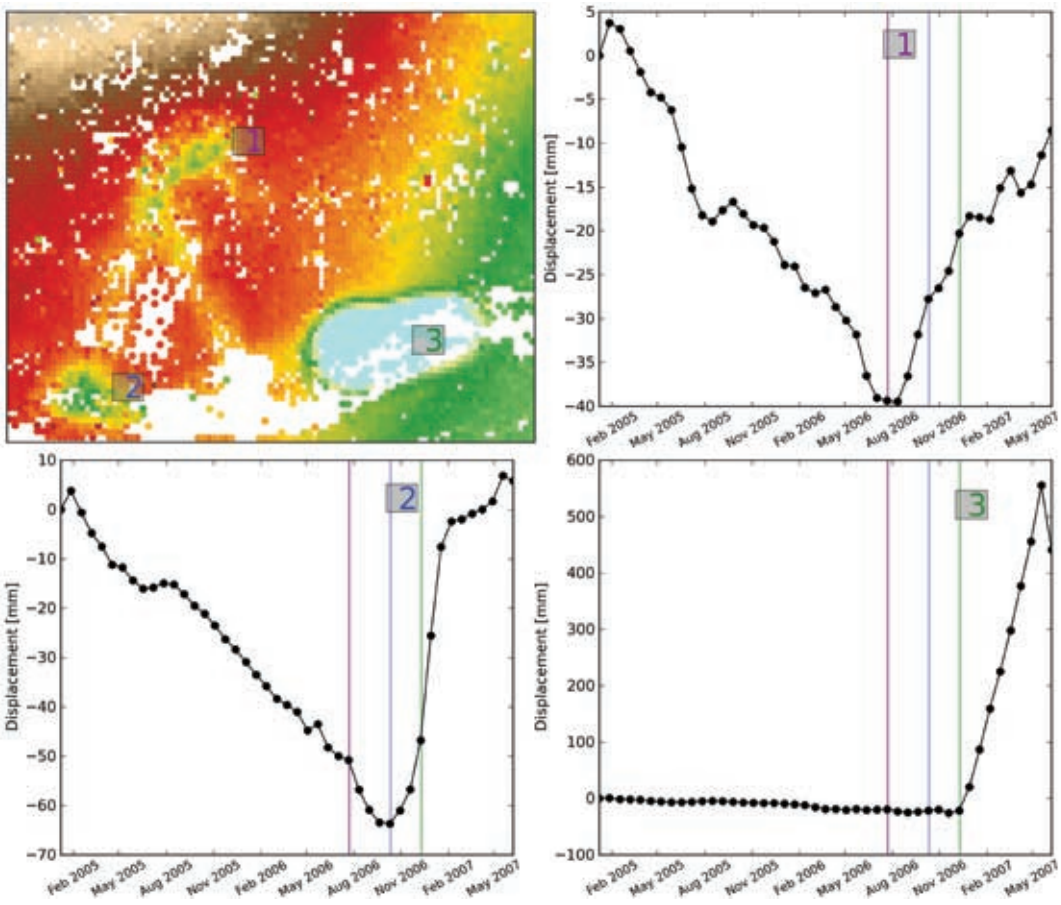

Figure 8 *An example of the time resolution of PSInSAR. For different parts of the 4.4 km x 3.6 km area: at upper left, the subsidence trend is reversed at different times. The three graphs are a time series for individual scatterers from the areas labelled 1, 2, and 3. The first area where the reversal of the subsidence is seen is denoted by the magenta 1, the next second by the blue 2, and the third by the green 3. Vertical lines are drawn in all time series to show the relative times when uplift started in each of the three areas.*

deviations for the vertical and horizontal components are at the moment under further investigation. The fact that GPS is more precise in the horizontal direction than in the vertical direction is well established. For InSAR data, on the other hand, the acquisition geometries should give very similar precision figures for both directions, at least theoretically.

Due to the small extent of the anomalies in the southeast of the field, GPS did not capture the uplift well in that area.

Geomechanical inversion

We are ultimately interested in changes in the reservoir rather than at the surface. We can establish a relationship between surface and subsurface using an analytical geomechanical model, in which the overburden is described as an anisotropic, homogeneous, linear-elastic, half-space. The anisotropy controls the ratio of vertical to horizontal displacement (i.e., a VTI medium in seismological terms).

Using this model we can perform an inversion to estimate the volumetric strain that caused the surface deformation. The inversion result is constrained so that the reservoir is assumed only to compact, i.e., all volumetric strains should be compressional, using a constrained least-squares inversion (e.g., Lawson and Hanson, 1974; Vogel, 2002). Kuvshinov (2007, 2008) shows that it is possible to

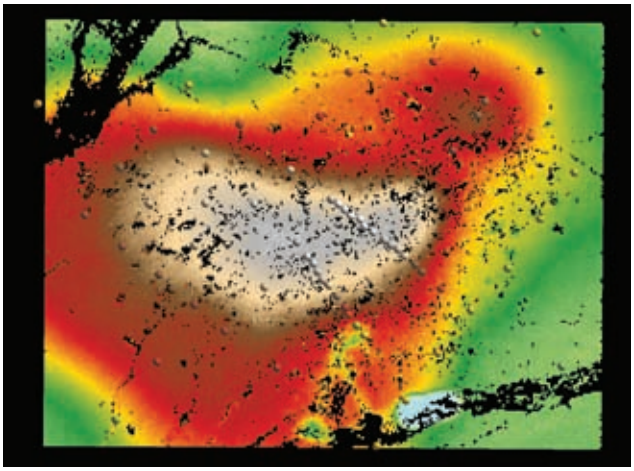

Figure 9 *Average vertical velocity estimates of GPS and PSInSAR displayed on the same map with the same colour scale as in Figures 4–6. The spheres denote GPS stations.*

calculate an analytic solution for a geomechanical model where the source of deformation is given by a nucleus of strain, integrated over a polyhedron. As we assume linear elasticity, the volumetric strain in the reservoir can be expressed in terms of pore pressure changes, if the uniaxial compaction coefficient is known and constant (e.g., Fjær et al., 2008). If the uniaxial compaction coefficient is unknown, or varying, we can nevertheless associate reservoir strain with 'pseudo-pressure', which needs further calibration. Spatial variability of the strain change is captured by forming the reservoir with a superposition of depleting blocks. For this reason we will use the terms strain change and (pseudo) pore pressure change interchangeably.

Figure 12 shows that the inversion results for vertical deformations fit the data quite well, as do the horizontal deformations. However, the residuals show a systematic underestimation of the vertical deformation, and a sys-

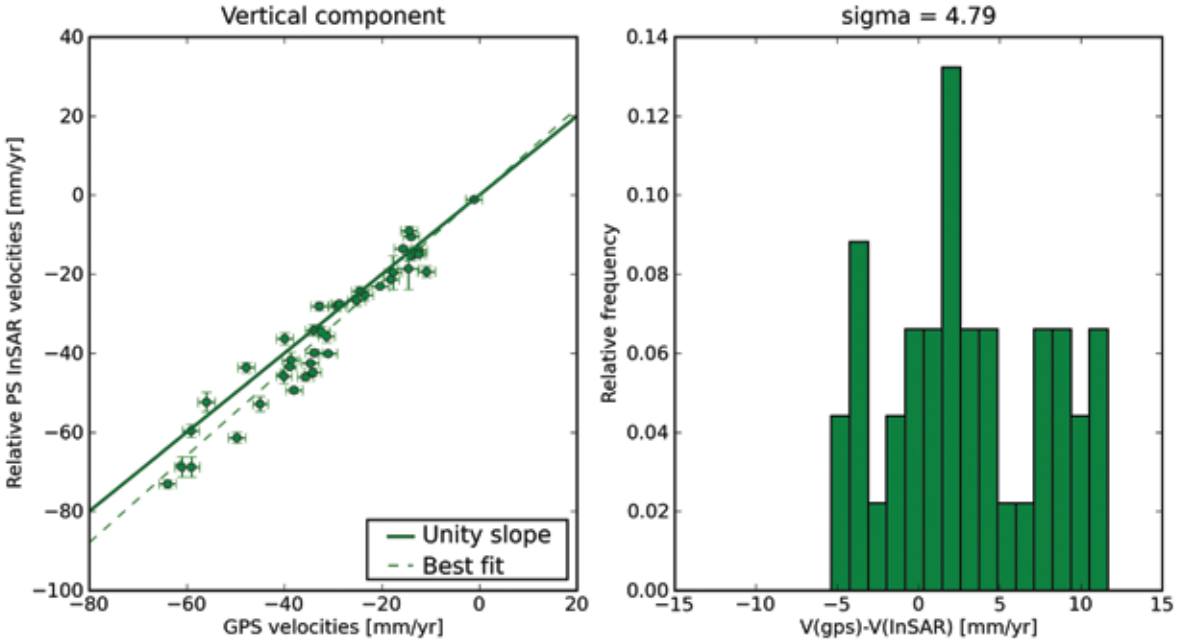

Figure 10 *Crossplot and histograms of the residuals of the vertical displacement estimates from PSInSAR and GPS. The subsidence estimates agree within 4.8 mm yr-1.*

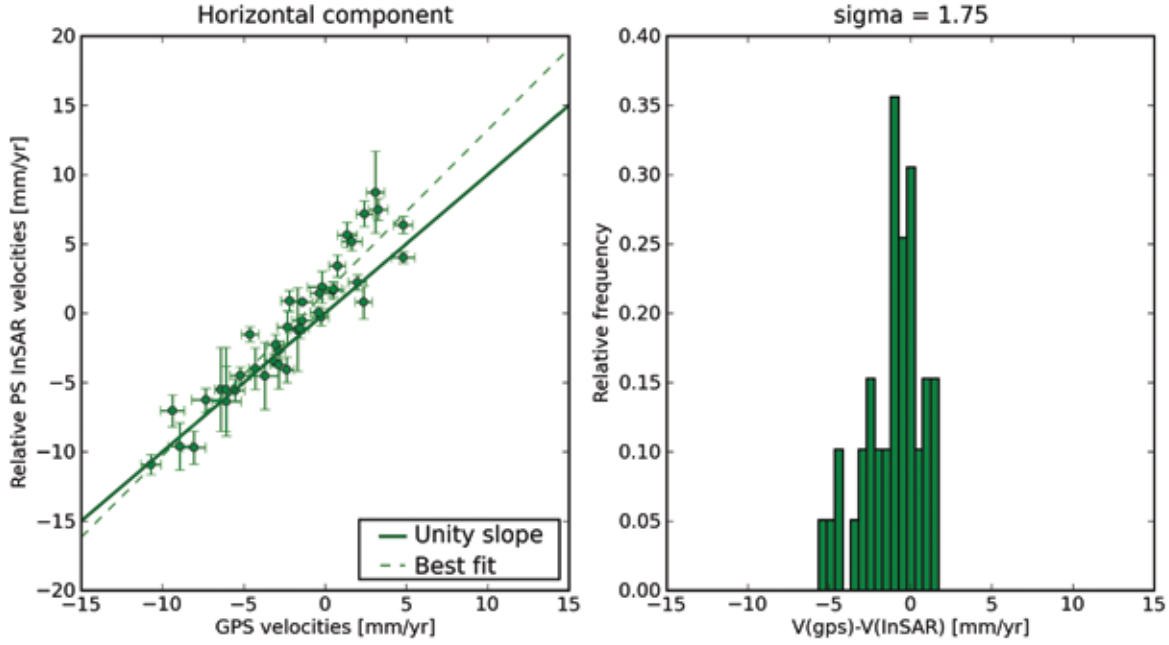

Figure 11 *Crossplot and histogram of the residuals of the horizontal displacement rates. The displacement rates agree within 1.8 mm yr-1.*

tematic overestimation of the horizontal deformation. The result shown is the best fit after an extensive search of the parameter space. This misfit only manifests itself after using both components of the displacement fields. The result of the inversion of the vertical components alone shows only random residuals at the noise level of the data. This can be seen as a manifestation of the fact that the model space is highly non-unique and that by inverting only the vertical data a large null-space of equivalent models in terms of data matching remains. This null space is constrained significantly by the horizontal data, in our case to the point that none of the geomechanical models that we considered were able to explain both components of the data. As can be seen in Figure 12, the residuals of the inversion contain a significant systematic component.

However, this fact is not too surprising because we have assumed a homogeneous half-space where the only source of deformation is given by compaction of the shallow reservoir. That is, we completely ignored the possible effects of the deeper reservoir and we completely ignored possible inhomogeneities or stiffness contrasts of the overburden.

In order to benchmark the reservoir level results of the inversion, we compared the reservoir changes as predicted from the inversion to a current estimate of pressure changes from a reservoir simulation. As can be seen in Figure 13, the areal distribution of reservoir strain matches quite well with the predicted reservoir pressure changes over the time in question.

Gradients and fault detection

The observation that the geomechanical model used in the inversion could only partially explain the data triggered a search for possible further information on inhomogeneities that might be contained in the data. In particular, the difference in slope of the subsidence bowl in different areas gave a strong indication that InSAR data can detect subsurface inhomogeneities.

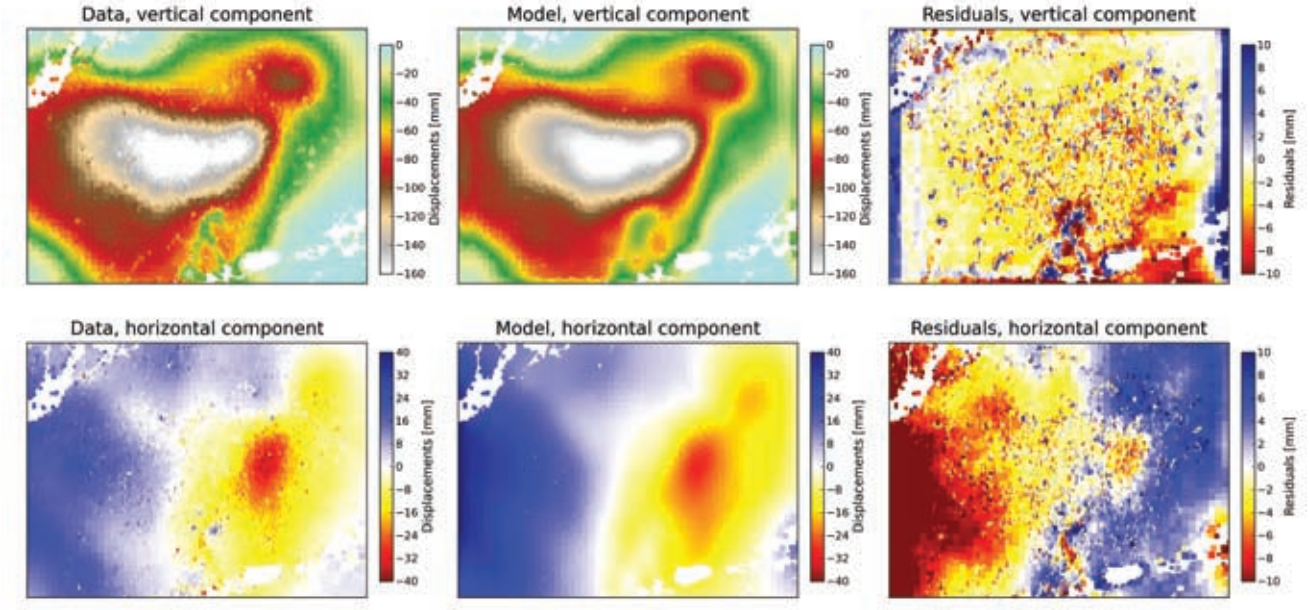

Figure 12 *Results of the combined inversion. Left panel – input data; middle panel – best-fit model; and right panel – residuals, (data-model). The top row shows the vertical component, and the lower row shows the horizontal component. The best-fit result overestimates horizontal deformation and underestimates the vertical component.*

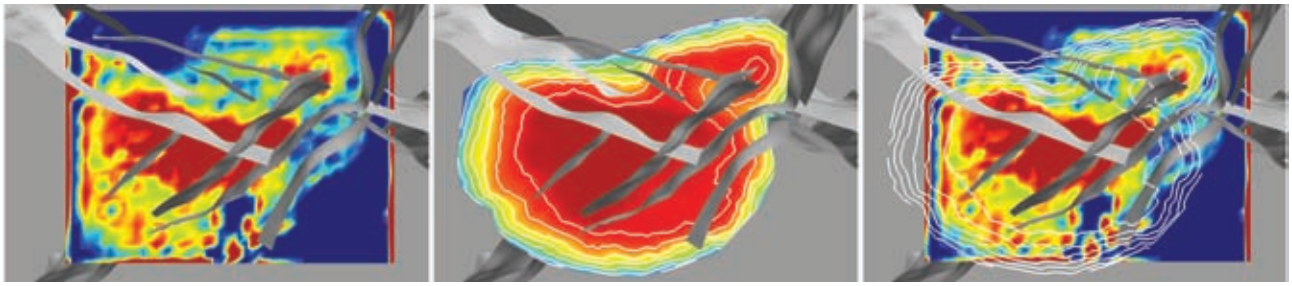

Figure 13 *Comparison of inversion pseudo-pressure changes and pressure change predictions from the reservoir simulator. Left panel – inversion results; middle panel – pressure change prediction of the reservoir simulation; and right panel - inversion results with contour lines of the pressure change predictions. Note the excellent agreement in extent in the north. The inversion area is clipped on the west and south sides as the data area was slightly too small to give reliable results outside the inverted area.*

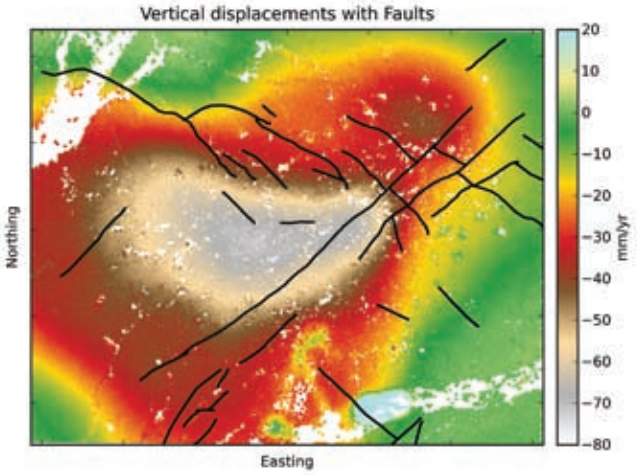

Figure 14 *Vertical InSAR data overlaid with faults interpreted at reservoir level. In the north-west, in particular, the steep flank of the subsidence bowl conforms remarkably well to the known faults at reservoir level.*

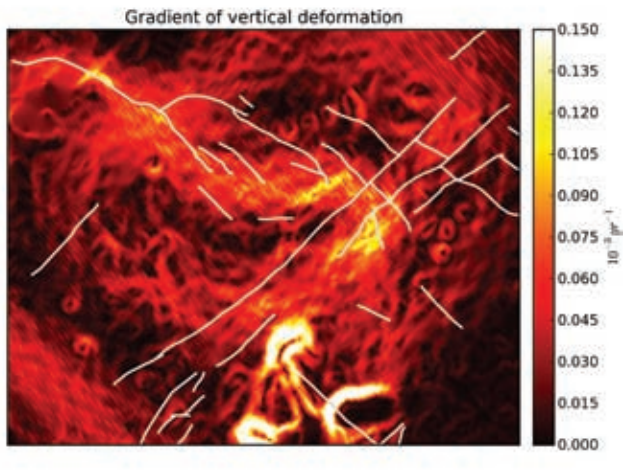

Figure 15 *Vertical displacement gradient shown together with the known fault systems. The areas with rapidly changing displacement rates seem to correspond well to the known faults.*

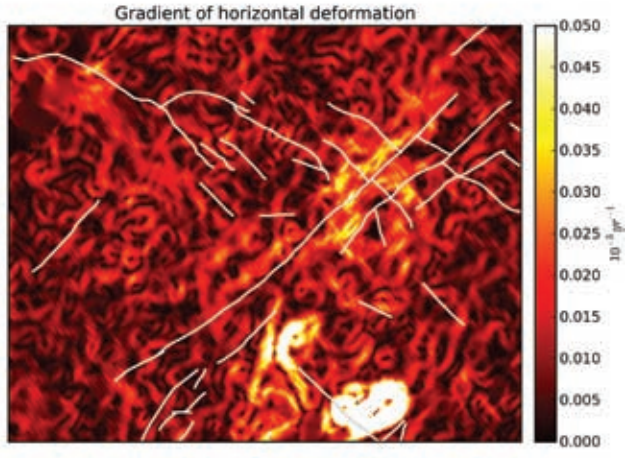

Figure 16 *Horizontal displacement gradient shown together with the known fault systems. The areas with rapidly changing displacement rates seem to correspond well to the known faults.*

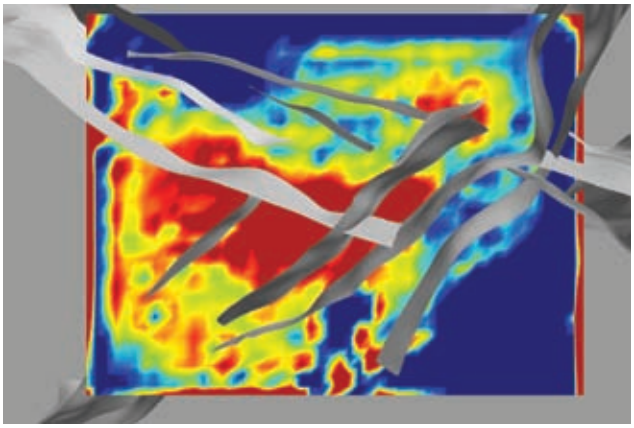

Figure 17 *Inversion result for reservoir strain from the combined inversion of the horizontal and vertical displacements at reservoir level. Also shown are some of the known major faults.*

The spatial distribution of the subsidence field shows some striking asymmetries, clearly visible in the SAR data. This is particularly evident looking into the shape of the displacement field towards the north and the east, where the subsidence bowl exhibits an abrupt change not present in the south and the southwest. As the field is heavily faulted, we have tried to understand if there is evidence that the known faults influence the shape of the subsidence bowl. Since faults are mapped out in the subsurface and the seismic data in the shallow section are of poor quality, this analysis has to remain qualitative, as it is difficult to determine how close the faults extend to the surface or their exact orientation. In Figure 14 the faults at the top reservoir are shown together with the InSAR data. In particular, the northwest edge of the subsidence bowl corresponds remarkably well with the fault line. It appears as if the northwestern extent of the subsidence bowl is bounded by the fault, as almost no subsidence is observed in the northwest. However, no clear correlation between the faults and the shape of the subsidence bowl can be established in the interior.

In order to understand the horizontal distribution of subsidence rate variations, the first quantity to consider – from a geomechanical point of view – is the strain tensor. However, as we only have access to two components of the displacement field, it is impossible to derive the strain tensor from the data. Therefore, we have to limit our analysis to the horizontal gradients. In particular, we consider the quantities:

$$\left|\left(\frac{\partial}{\partial x}+\frac{\partial}{\partial y}\right)u_z(x,y)\right| \text{ and } \left|\left(\frac{\partial}{\partial x}+\frac{\partial}{\partial y}\right)u_x(x,y)\right|,$$

where u_z and u_x are the vertical and horizontal components of displacement, respectively.

The faults delineated in Figures 15 and 16 were interpreted at top reservoir, at a depth of ~750m. As the faults are not necessarily vertical and their lateral extent may vary, relating surface deformation to fault features can

only be indicative. Nevertheless, the correlation between maximal vertical gradients and estimated fault location is quite striking, if we ignore the signals stemming from the rapidly changing inverted y in the southeast. Therefore, it seems possible to identify, at least qualitatively, faults governing the reservoir from InSAR data, although other prior information should be used in order to accurately estimate reservoir characteristics.

Figure 17 shows the result of the inversion together with major known faults. The sharp boundary of the subsidence bowl in the northwest and in the east coincides remarkably well with the delineated faults in these areas.

Conclusions

We have presented a study concerning the monitoring of vertical and horizontal surface deformation, using PSInSAR. The area of interest turned out to be favourable for the application of PSInSAR analysis and approximately 2400 and 3000 PS km^{-2} were identified for ascending and descending data respectively. A comparison with existing GPS data over the same field showed an agreement within 4.8 mm yr^{-1} (standard deviation) for the vertical component and 1.8 mm yr^{-1} for the horizontal component. Therefore, PSInSAR is suitable for monitoring surface deformation changes with high accuracy. The data showed an area with very strong surface uplift in a shallow region in the southeast of the field. The time-resolved nature of the data gave further insight into the temporal behaviour of this anomaly.

Inversion of the dataset with an analytical geomechanical model gives residuals at the level of the measurement noise if only one of the components of the data is considered. However, it shows systematic residuals if both vertical and horizontal components are inverted at the same time. This fact demonstrates that the deformation data of one component can be fitted by a large family of geomechanical models. The estimation of two components of the displacement field, which can be done by properly combining two InSAR datastacks, significantly constrains the family of geomechanical models that acceptably fit the observations.

By comparing the PSInSAR data with the known faults at reservoir level, an intriguing correlation is evident between the known fault system and the gradient of the subsidence field. Furthermore, the inversion result also seems, in some areas, to be bounded by the known faults. A comparison with the pressure change maps from the reservoir simulation over the time in question shows a good areal agreement between the predicted and estimated pressure changes. A more quantitative close-the-loop exercise to incorporate the insights from the inversion results into the reservoir model is required for further analysis.

Acknowledgements

The authors thank the Ministry of Oil and Gas, Oman for permission to publish this work. We also thank Fredrik Hansteen, Samantha Grandi, Neil Hodgson and Stephen Bourne for stimulating discussions, Latifa Qobi for the pressure maps, and T. Herring for the GPS analysis. PSInSAR is an international trademark of Politecnico di Milano, licensed to TRE.

References

Ferretti, A., Prati, C. and Rocca, F. [2001] Permanent Scatterers in SAR interferometry, *IEEE Transactions on Geoscience and Remote Sensing*, **39**, 8-20.

Fjær, E., Holt, R.M., Horsrud, P., Raaen, A.M. and Risnes, P. [2008] *Petroleum Related Rock Mechanics*, 2nd Edition. Elsevier, Amsterdam.

Hanssen, R.F. [2001] *Radar Interferometry*, Kluwer, Dordrecht.

Herring, T.A. [1999] Geodetic applications of GPS. *Proceedings of the IEEE,* **87**(1), 92–110.

Herring, T.A. [2003] MATLAB tools for viewing GPS velocities and time series. *GPS Solutions,* **7**, 194-199.

van der Kooij, M. and Mayer, D. [2002] The application of satellite radar interferometry to subsidence monitoring in the Belridge and Lost Hills fields, California. *IEEE Geoscience and Remote Sensing Symposium*, *IGARSS '02*, **1**, 201-202.

Kuvshinov, B.N. [2007] Reflectivity method for geomechanical equilibria. *Geophysical Journal International*, **170,** 567-579.

Kuvshinov, B.N. [2008] Elastic and piezoelectric fields due to polyhedral inclusions. *International Journal of Solids and Structures*, **45**, 1352-1384.

Lawson, C.L. and Hanson, R.J. [1974] *Solving Least Squares Problems*. Prentice-Hall, Upper Saddle River, New Jersey.

Madsen, S.N. and Zebker, H.N. [1998] Imaging radar interferometry. In: Henderson, F.M. and Lewis, A.J. (Eds.) *Principles and Applications of Imaging Radar*, 3rd Edition. John Wiley & Sons, New York.

Maron, K.P., Bourne, S., Klemm, H., van den Beukel, A. and McGillivray, P. [2008] Insights from monitoring of heavy oil production in Peace River, Canada. *Abu Dhabi International Petroleum Exhibition and Conference*, SPE 118244.

Patzek, T.W. and Silin, D.B. [2000] Use of INSAR in surveillance and control of a large field project. *21st Annual International Energy Agency Symposium, Edinburgh*.

Patzek, T.W., Silin, D.B. and Fielding, E. [2001] Use of satellite radar images in surveillance and control of two giant oilfields in California. *SPE Annual Technical Conference and Exhibition*, New Orleans, SPE 71610.

Raikes, S., Mathieson, A. and Roberts, D. [2008] Integration of 3D seismic with satellite imagery at In Salah CO2 Sequestration Project, Algeria. *78th SEG Annual Meeting*, Expanded Abstracts, **27**, 2856-2858.

Vasco, D.W. , Ferretti, A. and Novali, F. [2008] Estimating permeability from quasi-static deformation: temporal variations and arrival-time inversion. *Geophysics*, **73**, 37–52.

Vogel, C.R. [2002] *Computational Methods for Inverse Problems*. SIAM, Philadelphia.

Received 17 December 2009; accepted 26 February 2010.

